Korean J. Chem. Eng., 38(8), 1566-1577 (2021)
DOI: 10.1007/s11814-021-0804-6

pISSN: 0256-1115
eISSN: 1975-7220

Development of augmented virtual reality-based operator training system for accident prevention in a refinery

Changjun Ko*, Hodong Lee*, Youngsub Lim,***,†, and Won Bo Lee*,†**

*School of Chemical and Biological Engineering, Seoul National University, Gwanak-ro 1, Gwanak-gu, Seoul 08826, Korea
**Department of Naval Architecture and Ocean Engineering, Seoul National University, Gwanak-ro 1, Gwanak-gu, Seoul 08826, Korea
***Research Institute of Marine Systems Engineering, Seoul National University, 1 Gwanak-ro, Gwanak-gu, Seoul 08826, Korea
(*Received 30 December 2020 • Revised 29 March 2021 • Accepted 11 April 2021*)

Abstract−A new operator training system that trains both control room and field operators by coupling dynamic processes and accident simulations, thereby preventing potential hazards in a chemical plant, is proposed. The two types of operators were trained in different training environments — a conventional distributed control system interface for the control room operators and an augmented virtual reality-based system for the field operators. To provide quantitative process changes and accident information driven by the actions of the trainees in real time, two types of simulation, dynamic processes and accidents, were implemented. The former was accomplished through a real-time dynamic process simulation using Aspen HYSYS; the latter was achieved by replacing the high-accuracy accident simulation model based on computational fluid dynamics with a variational autoencoder with deep convolutional layers and a deep neural network surrogate model. The resulting two types of outcomes were transferred across each training environment in a platform called the process and accident interactive simulation engine using object linking and embedding technology. In the last step, an augmented virtual reality-based platform was attached to the process and accident interactive simulation engine, making communication between the control room and field operators possible in the proposed operator training system platform.

Keywords: Potential Hazards, Operator Training System, Dynamic Process Simulation, Computational Fluid Dynamics, Variational Autoencoder with Deep Convolutional Neural Layers, Augmented Virtual Reality

INTRODUCTION

Although the advancement of the chemical industry has brought significant benefits to society, the increased scale of chemical processes has also given rise to potential risks. Today, as processes become more complex, the hazard of an accident and damage is growing as well. For instance, the explosion accident on March 23, 2005 at the British Petroleum refinery in Texas caused 195 casualties. According to the investigation report, inappropriate training for the operations personnel in advance was considered as the main reason for the accident [1]. In other studies, the main reason for accidents in plants has been identified as the incorrect operation of process units by operators owing to a lack of previous training [2], accompanied by lack of relevant knowledge of the process [3], resulting in a large number of man-made disasters.

For quite some time, many people in the chemical industry have been trying to solve these problems. They mostly focused on reducing accident damage by properly educating operators on how to respond in emergency situations [4,5]. This idea has resulted in an increase in the size of the operator training system (OTS) manufacturing market [6], and accordingly, remarkable developments have been made in the related field. Early OTSs mainly focused mainly on dynamic process simulations [7-10] such as UniSim® by Honeywell and Aspen® by AspenTech. On these platforms, training scenarios usually start with upsets of process variables such as temperature, pressure, and flow rate due to adverse events in one or more process unit. When these scenarios evolve, trainees are advised to take appropriate actions to bring those upsets back to normal states. These OTSs are used to educate control room operators (CROPs) and contribute greatly to improving the coping ability of operators in emergency situations. However, these types of process-simulation-based OTSs have limitations in educating field operators (FOPs) because accidents such as leaks, fires, and explosions are excluded in training scenarios.

Because agile cooperation between CROPs and FOPs is crucial in real accident situations [11], efforts have been made in recent years to combine the results of accident simulation with dynamic process simulation, and furthermore with virtual reality (VR). Cha et al. developed a training program in VR that computed the fire effect using computational fluid dynamics (CFD) [12]. Schneider Electric tried to map the visual effect of fire onto VR using the EYESIM® platform, wherein process simulation results are mapped and displayed in real time in VR [13]. These methodologies try to solve the integration problem of the existing dynamic simulation and accident simulation, but the results have not been effective. Therefore, to connect process simulation with accident simulation,

†To whom correspondence should be addressed.
E-mail: s98thesb@snu.ac.kr, wblee@snu.ac.kr

Manca et al. introduced augmented virtual reality (AVR) as a solution wherein additional process information such as pressure, temperature, and flow rate is imbedded to the VR by integrating the process simulator of UniSim® with the self-developed accident simulator of AXIM [14]. In addition, they used the objective linking and embedding (OLE) technique to effectively connect the results of the two modules. As a result, they succeeded in creating a pioneering AVR-based training platform by mapping the two-dimensional pool fire accident simulation results to VR. However, this method has a limitation in that it is based on simple parametric two-dimensional accident results, making it difficult to yield quite accurate three-dimensional accident information that is to be supplied to trainees.

When estimating accident results, CFD, which can consider various terrain conditions and fluid characteristics, has been the most widely used simulation tool in recent years. There are various models such as dispersion, fire, and explosion in CFD, and many types of commercial CFD tools are currently being produced and used by various organizations [15-17]. Nevertheless, CFD models have a critical drawback: the computation time. Most CFD tools take more than an hour to compute the results [18]. However, accident result data provided to the VR should be calculated very quickly, because the accident consequence is changed by the action of the trainee almost in real time. For example, the size of the gas cloud generated by a leakage accident changes in real time depending on how quickly the training center shuts off the block valve near the leakage accident. For this reason, CFD could not be applied to AVR-based OTS, which requires rapid calculation. To solve this problem, studies on surrogate models that can simply express complex structures of a certain model have been conducted. Palmer et al. used Gaussian process regression (GPR) meta models to optimize an ammonia synthesis plant [19]. Chen et al. expanded the domain of meta-models to time-space-dependent output variables in connection with GPR [20]. Widodo et al. used support vector machine in machine condition monitoring and fault diagnosis, and Fauvel et al. adopted a spatial-spectral kernel-based approach for the classification of remote-sensing images [21,22].

However, the above-mentioned studies built only relatively simple models with only a small number of input and output variables, the results of which were not sufficient to generate information to be provided to trainees moving in a large virtual environment. In addition, support vector machine algorithm and kernel-based learning are not suitable for nonlinear and complex data sets. Therefore, a model that can address large data and numerous input and output variables is essential to applying big data-based machine learning techniques to chemical processes [23]. According to various studies that deal with meta-modeling [24], dimensionality reduction is an essential factor because the huge size and complexity of the data makes analysis difficult. Autoencoders (AEs) are one of the possible techniques since they can provide nonlinear transformation conducted by the nonlinear activation functions and multiple layers. In addition, when convolutional neural networks (CNNs) are combined with AEs, a significant improvement on model performance can be shown [25,26]. Furthermore, a new methodology of variational AEs (VAEs) that introduces the latent space concept generated by features of the training set has been developed as a powerful model [27]. In particular, Na et al. combined a VAE with deep CNNs and demonstrated excellent improvement in performance [28].

After performing dimensionality reduction, a regression process that can express the correlation between input and output is necessary. Recently, deep neural networks (DNNs) with multiple hidden layers have shown great performance improvement with the resolution of vanishing and exploding gradients, overfitting, and low learning rates [29]. Ioffe et al. proposed batch normalization (BN) to further address the vanishing and exploding gradient problem [30]. Finally, numerous optimization algorithms such as momentum optimization, Nesterov Accelerated Gradient, AdaGrad, RMSProp, and Adam Optimization have been proposed to effectively estimate the weight parameters of neural networks, to be highly likely to obtain high-performance surrogate models [31,32].

Herein, we develop an AVR-based OTS for the heavy oil desulfurization (HOD) process. To provide trainees process and accident information that is coupled with each other, process simulation and accident simulation are carried out using the commercial software Aspen HYSYS and FLACS, respectively. Thereafter, a surrogate model with respect to jet fire in FLACS is constructed by random sampling of processed data for real-time application of CFD-based surrogate model to the AVR-based target OTS platform. To build the proposed surrogate model, the input is defined as wind speed, wind direction, release duration, and time step and the outputs are defined as total heat flux at each grid in three-dimensional space. First, output is compressed using a VAE with deep convolutional layers (VAEDC) and secondly, the relationship between the input and the output is estimated using a DNN. The performance of the newly constructed model is compared with that of other commonly used models to evaluate the performance improvement. Finally, the proposed model, which can calculate output from any input in a sub-second, is demonstrated to show that a tool to bridge accident results not only with dynamic process results but also with VR is successfully manufactured.

STRUCTURE OF OTS PLATFORM

1. Structure of Proposed OTS with AVR

As described in the previous section, to train both CROPs and FOPs simultaneously, the coupling between process and accident simulations is indispensable. The structure of the proposed OTS is displayed in Fig. 1. There are two main platforms in the structure: a distributed control system (DCS) platform and an AVR platform. The DCS platform, called the process and accident interactive simulation engine (PAISE), serves as providing process information to CROPs; therefore, the real-time trend of the process variables can be seen in the DCS platform while the AVR platform serves to providing accident information to FOPs.

In this study, an abnormal pressure rise that brings about a gas release and subsequent jet fire is demonstrated as the representative training process. When the training scenario begins, the process variables such as temperature, pressure, and flow rate are calculated according to predetermined conditions by Aspen HYSYS. These values are transferred to the DCS platform to calculate the release rate using a discharge equation, which is the input of the accident

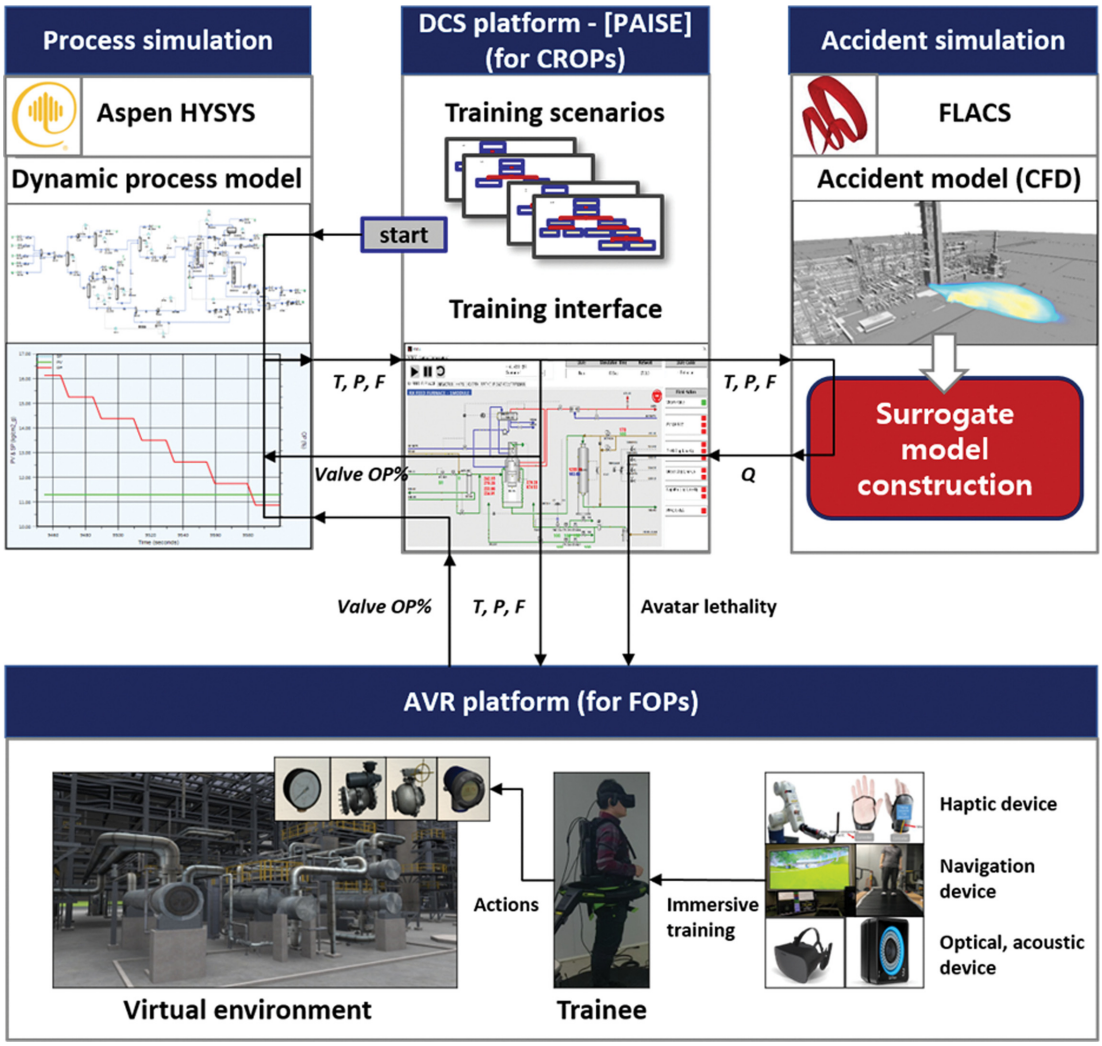

Fig. 1. Structure of proposed AVR-based OTS.

model.

$$\text{Release rate} = C_{disc} A \sqrt{\gamma \rho P \left(\frac{2}{\gamma}+1\right)^{\frac{\gamma+1}{\gamma-1}}} \quad (1)$$

where C_{disc}, A, γ, ρ, and P denote the discharge coefficient, hole area, specific heat ratio, fluid density, and pressure, respectively. With the calculated release rate, a CFD-based jet fire accident is simulated using FLACS V10.7r1. The heat flux (Q) data are obtained as simulation output at each grid of three-dimensional space.

However, since the CFD-based accident model takes a long time to calculate the results, therefore, data cannot be provided in real time with this method. The solution to this obstacle is to build a surrogate model that can replace the CFD-based jet fire accident model with the same input and output, of which the details are provided in the later section. After the CFD-based model is replaced by the surrogate model, the output values of heat flux are transferred to the AVR platform. In the AVR platform, additional equipment such as haptic, navigation, optical, and acoustic devices are attached to escalate the vivid training atmosphere and provide improved training effects to trainees.

2. Target Process and Outline of Training Scheme

The HOD process has a critical role in the petrochemical process. It aims to remove residue sulfur in atmospheric residue oil using a reaction with hydrogen, as expressed below:

$$R_2CHSH + H_2 \xrightarrow[Catalyst]{} R_2CH_2 + H_2S \quad (2)$$

$$\text{Thiophene} + 4H_2 \xrightarrow[Catalyst]{} \text{Paraffin} + H_2S \quad (3)$$

The reaction occurs with five reactors in series, as indicated in Fig. 2(a). These reactors are operated under harsh conditions of approximately 180 barg and 360 °C, of which the detailed information is listed in Table 1. These extreme operating conditions lead to a high likelihood of accidents, such as release and fire, resulting in massive damage. For these high potential risks, it is critical to educate operators to take appropriate measures in the case of accidents, thereby minimizing the physical and economic damage to the plant. The most probable abnormal situation by the hazard and operability report from the licensing company is process upsets derived from equipment failure that controls the pressure, such as

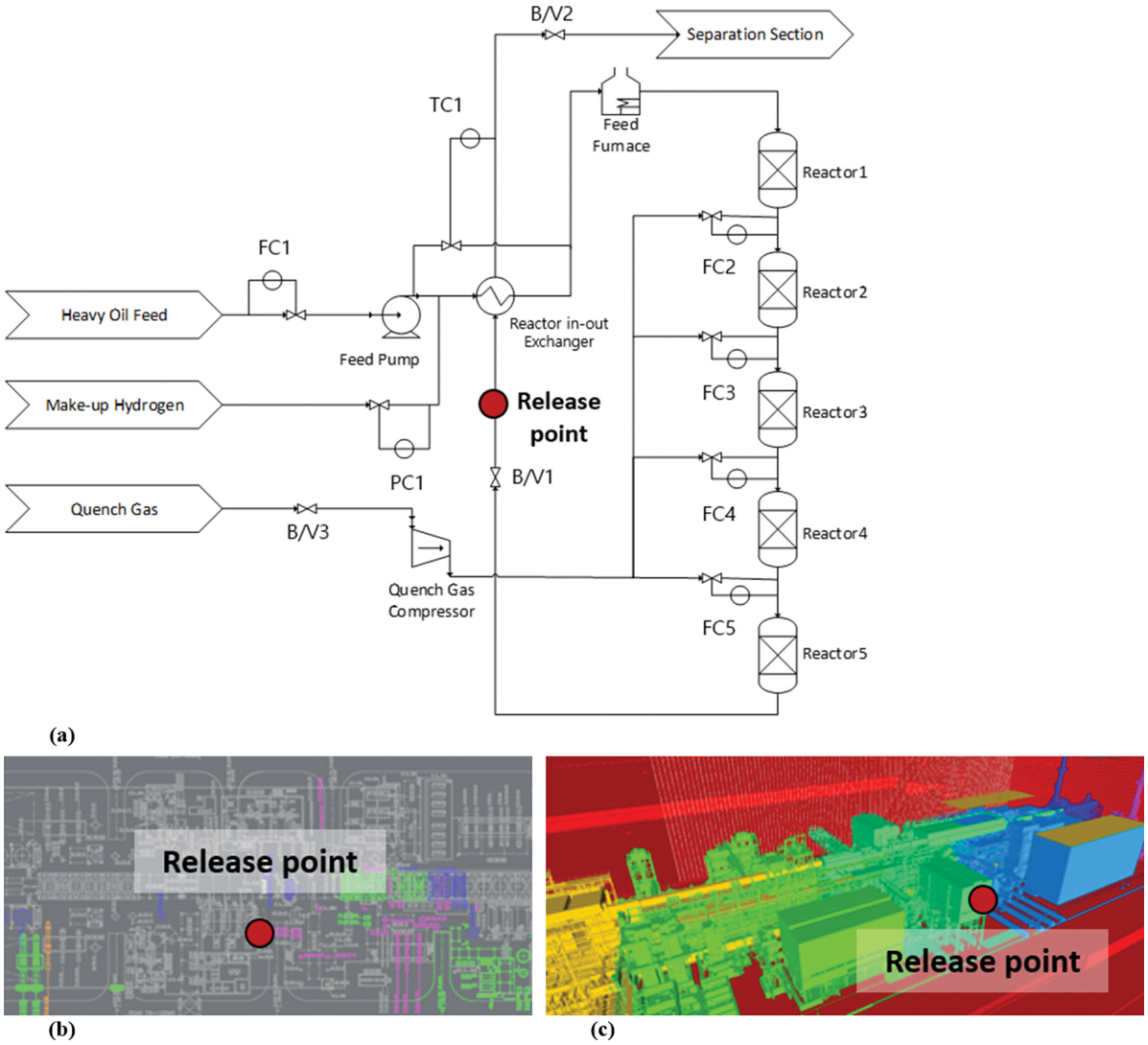

Fig. 2. Layout and geometry of HOD process. (a) Process flow diagram, (b) plot plan, (c) 3D view of CAD image in FLACS.

Table 1. Steady-state operating conditions of the reactors

Unit description	Pressure (barg)	Temperature (°C)	Flow (10^4 kg/h)
Reactor 1	192.4	388.1	2.381
Reactor 2	191.6	385.4	2.403
Reactor 3	186.4	382.7	2.435
Reactor 4	181.1	381.8	2.473
Reactor 5	175.6	380.2	2.494

compressor failure. When initiated, pressurized hydrogen can bring about a release of hydrogen and light hydrocarbon gases through pipeline flanges near the reactor, which is operated under the extreme conditions mentioned above, and subsequently cause jet fire. This accident could propagate throughout the plant and result in a massive calamity. Therefore, a sequence of process upsets and accidents are modeled for the training scenario. As described in the previous section, process upsets are modeled by Aspen HYSYS according to predefined conditions to provide the trainees with almost the same process variable trends as in case of a real situation. The physical and thermodynamic conditions are computed by the modified Peng-Robinson state model equation [33]. When the upset scenario is initiated, a simple pressure-flow equation is used additionally to compute the changed conditions of the process variables.

$$\text{Flow} = K\sqrt{\Delta P} \tag{4}$$

where K and ΔP denote the conductance of a certain pressure node, such as a valve or heat exchanger, and the change in pressure across the node, respectively. As errors are accumulated, the process variables attain predefined release conditions at certain points, and the release rate is calculated by Eq. (1). The obtained release rate is used as an input for the jet fire accident model.

3. Accident Data Preparation

The jet fire scenario is modeled by FLACS to provide the sufficient samples to generate a surrogate model. The size of the entire simulation domain is 50 m, 50 m, and 30 m in the x, y, and z

Table 2. Accident scenario conditions

Variable	Value
Ambient temperature	25 °C
Ambient pressure	1 bar
Wind direction	0-2π
Wind speed	0.5-5 m/s
Discharge rate	14.4 kg/s
Release duration	60-180 s
Pasquill class	None
Total simulation time	180 s

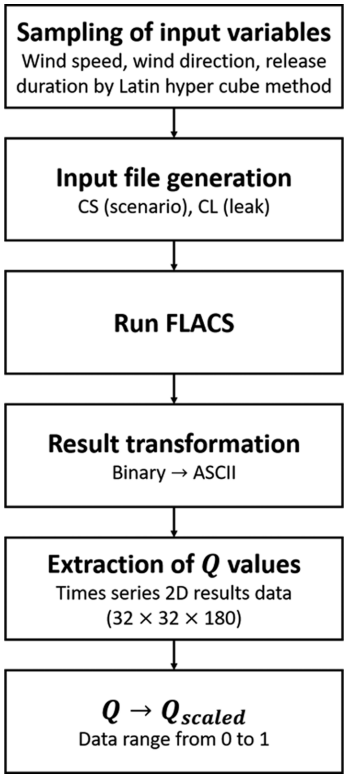

Fig. 3. Flow chart of data processing.

directions, respectively, with a uniform grid of 1.6 m. The location of the release point is marked in Fig. 2(a), 2(b), and 2(c). The simulation inputs are selected to create discrete outputs. The other simulation conditions are shown in Table 2.

The entire process of training is indicated in Fig. 3. First, the three input variables of wind speed, wind direction, and release duration are randomly sampled using the Latin hypercube method [34]. FLACS input files CS (scenario) and CL (leak) are generated using these variables, and 785 cases in total are simulated to obtain data points for training. The resulting data are acquired in the form of binary files and transformed to American Standard Code for Information Interchange (ASCII) files for post-processing. From the ASCII files, the Q values (28×28×180), of which the dimensions match the number of x, y coordinates, and time steps, respectively, are extracted. Because the height that has the greatest impact on a person is near 2 m, the Q values of z coordinates at 1.6 m are

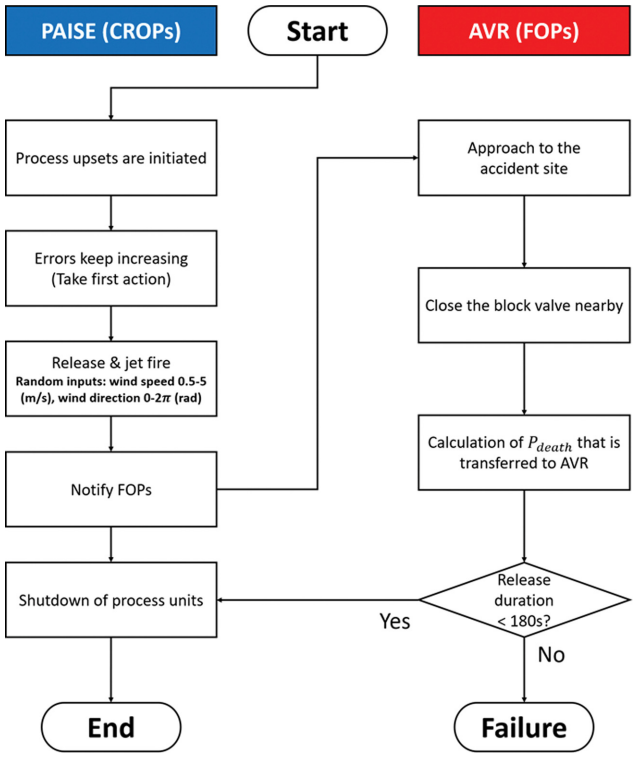

Fig. 4. Training scenario by communication of CROPs and FOPs.

used and other Q values of z coordinates are abandoned. In the last step, the data are shifted and rescaled to the range [0,1] using the following Eq. (5):

$$Q_{scaled} = \frac{Q - Q_{min}}{Q_{max} - Q_{min}} \tag{5}$$

where Q_{max} and Q_{min} denote the maximum and minimum Q values among the original samples.

TRAINING SCHEME

1. Definition of Training Scenario

As described in Section 2.1., the dynamic process simulation and accident data (Q) from the VAEDC-DNN surrogate model must be coupled in the AVR-based OTS for appropriate communication between the CROPs and FOPs. The representative training scenario in Fig. 4 indicates the sequence of the training and the configuration of how the process and accident models function interactively. The training procedure is accelerated for quick evaluation, which gives trainees relatively short 180 s for actions to be taken.

I. When the training scenario begins, process upsets are initiated by the quench gas compressor failure, and the results of the process variable changes are obtained by a dynamic process simulation.

II. All controllers (FC1-5, TC1, and PC1) are set to the manual mode and the CROPs are directed to take the first action, which is to manipulate the actuators (valves) manually to prevent the upsets from propagating further. However, even if they take the proper actions, errors continue to increase according to the predefined train-

ing scenario.

III. When the errors attain the predefined threshold, a gas release and subsequent jet fire occurs. The CROPs are directed to notify the FOPs of the accident site and initiate the shut-down procedure of the actuators (valves) in DCS. Further dynamic simulations are conducted accordingly.

IV. Upon receiving the order from the CROPs, the FOPs approach the accident site and close the block valve.

V. If the FOPs report to the CROPs that the action has been taken, the training ends.

For each training, when a jet fire occurs, the accident effect of Q is calculated in real time by the pre-trained surrogate model with two randomly selected input variables and one fixed input variable: wind speed (0.5-5 m/s), wind direction (0-2π rad), and release duration (180 s). When the FOPs approach the accident site in AVR, the information, e.g., x, y, and t, which denotes the Cartesian coordinates of the FOPs and time step in the virtual environment, is transferred to PAISE using OLE technology as in Fig. 1 [35]. With the x, y, and t information from the AVR and Q from the surrogate model, the lethality of the FOPs can be calculated with the simplified following radiation equations with the assumption that because the trainee is sufficiently close to the radiation source (jet fire), the effect of convection is negligible [36].

$$L_{rad}=\int_{t_0}^{t}\left(\frac{Q(x,y,t)}{\text{Area of unit grid}}\right)^{\frac{4}{3}}dt \tag{6}$$

where L_{rad} denotes the radiation dose, and t_0 is the initial time step when the jet fire first occurs [36].

$$Pr=-36.38+2.56\times\ln(L_{rad}) \tag{7}$$

$$P_{death}=\frac{1}{2}\left\{1+\text{erf}\left[\frac{Pr-5}{\sqrt{2}}\right]\right\} \tag{8}$$

Pr denotes the radiation probit and P_{death} the lethality of the trainee in the AVR. The calculated result can be transferred to the AVR using OLE technology in real time. When the FOPs close the block valve in AVR, the decreasing effect of the jet fire is recalculated by the surrogate model with the inputs of the original wind speed, wind direction, and new release duration as follows:

$$\text{Release duration}=t_{action}-t_0 \tag{9}$$

where t_{action} represents the time step when the FOPs close the block valve in AVR. The lethality of the FOPs in AVR is updated with the newly calculated accident result. If the release duration is greater than 180 s, which is the predefined maximum allowable time to act, the training scenario ends in failure. Otherwise, the information of the jet fire accident is provided to the FOPs in real time throughout the entire training procedure, making appropriate communication with CROPs possible.

2. Dynamic Process Simulation Modeling

The process model is constructed based on the information displayed in Fig. 2(a) by Aspen HYSYS. The goal is to simulate the change in process variables over time as the training scenario evolves. Accordingly, based on the steady state model, modeling of the dynamic process simulation is implemented. Sizing information, which is an essential element of dynamic process simulation, is obtained from the process flow diagram (PFD) and piping and instrumentation diagram (P&ID) from the licensing company. In addition, proportional-integral (PI) controllers are used for control logic realization based on the PI Eq. (10):

Table 3. Tuning parameters of PI controllers

System	K_c	τ_i
Flow	0.1	0.2
Pressure	2	2
Temperature	1	20

$$OP(t)=K_c\left(E(t)+\frac{1}{\tau_i}\int E(t)dt\right) \tag{10}$$

where OP(t) denotes the controller output value and E(t) error between the controller setpoint and process variable. K_c and τ_i are tuning parameters that represent the controller gain and integral time, respectively. The tuning parameters for removing the disturbance of the process are set to the general values, as indicated in Table 3.

3. Accident Simulation Modeling

Inputs and outputs are to be defined prior to the training procedure. As described in Section 2.4, the input to the original CFD model is wind speed (m/s), wind direction (rad), and release duration (s). In addition, one more input of time step (s) is added to the input to take into account of times series, resulting in a four-dimensional input space denoted as $v\in\mathbb{R}^{1\times4}$. The output of the surrogate model is two-dimensional contour images of Q_{scaled} denoted as $x\in\mathbb{R}^{28\times28}$ as described in Section 2.3. The goal of the surrogate model is to map the input space v to the output space x using data points by FLACS calculation. To accomplish high performance, the model is constructed of two parts: a VAEDC and a DNN. The function of the VAEDC is to compress and reconstruct the data and the DNN is to generate a regression model with the compressed data. The computing process of a neuron in each layer can be expressed as follows [37]:

$$Y_{i,j,k}=b_k+\Sigma\Sigma\Sigma y_{i',j',k'}w_{u,v,k',k} \tag{11}$$

where Y, b, y, and w denote the output of the neuron, bias term, input of neuron, and connection weight, respectively. Of the total 800 data points, 720 samples are used as the training set (v^{train}, x^{train}), and 80 samples are used as the test set (v^{test}, x^{test}) to assess the trained result. Since the number of data set is small, ten-fold cross validation method is implemented. Namely, the samples are randomly split into ten distinct subsets called folds, then the training model picks a different test fold for evaluation every time and training on the other nine folds. Fig. 5(a) and 5(b) displays the structure of VAEDC and DNN respectively. The detailed information of the proposed VAEDC-DNN model was introduced in the previous research [38].

The performance of the proposed model is compared with that of other models based on AEs and neural networks (NNs): NN with a simple AE (AE-NN), NN and DNN with deep convolutional AE (DCAE-NN, DCAE-DNN), DNN with a simple VAE (VAE-DNN), and DNN with VAEDC (VAEDC-DNN). The detailed information of each model is specified in Table 4.

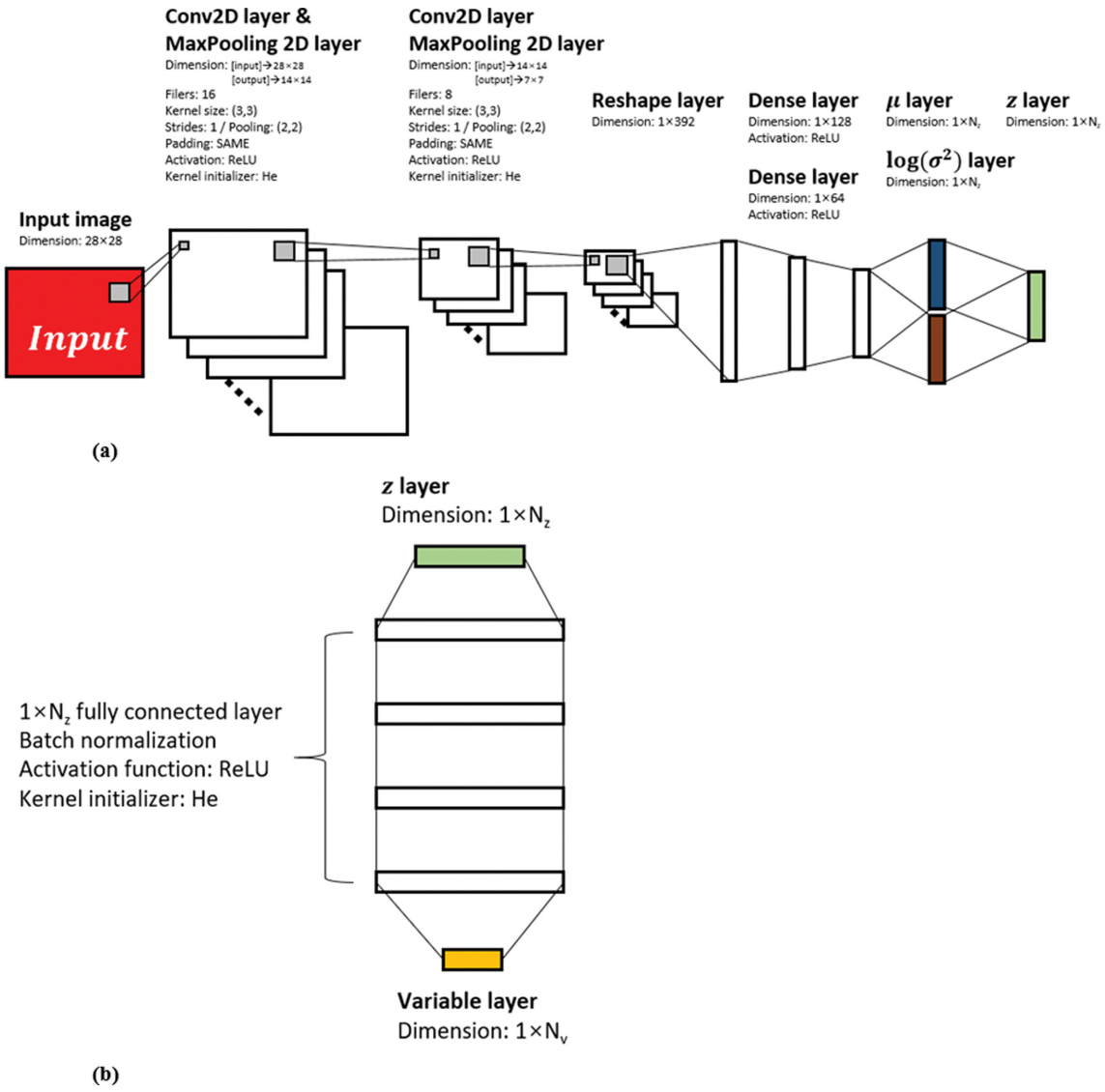

Fig. 5. Structure of VAEDC-DNN surrogate model. (a) Structure of VAEDC encoding part, (b) structure of DNN.

Table 4. Different surrogate models for comparison of VAEDC-DNN model performance

	AE-NN	DAE-NN	DAE-DNN	DCAE-NN	DCAE-DNN	VAE-DNN	VAEDC-DNN
Dimensionality reduction part description	One fully connected dense layer	5 Fully connected hidden layers		5 Fully connected hidden layers, 2 convolutional layers with max pooling		5 Dense layers with one variational layer	7 Fully connected hidden layers, 2 convolutional layers with max pooling
Loss function	Binary cross entropy					Variational lower bound	
Regression part description	NN	NN	DNN	NN	DNN	DNN	DNN
Loss function	Mean squared error						

RESULTS AND DISCUSSION

1. Dynamic Process Modeling Results

Fig. 6 displays the results of the dynamic process simulation at the location of block valve 1 (B/V 1). The simulation was accelerated eight times faster than the actual situation for rapid training. When training was initiated, physical and thermodynamic calculations were conducted according to the predefined scenario in

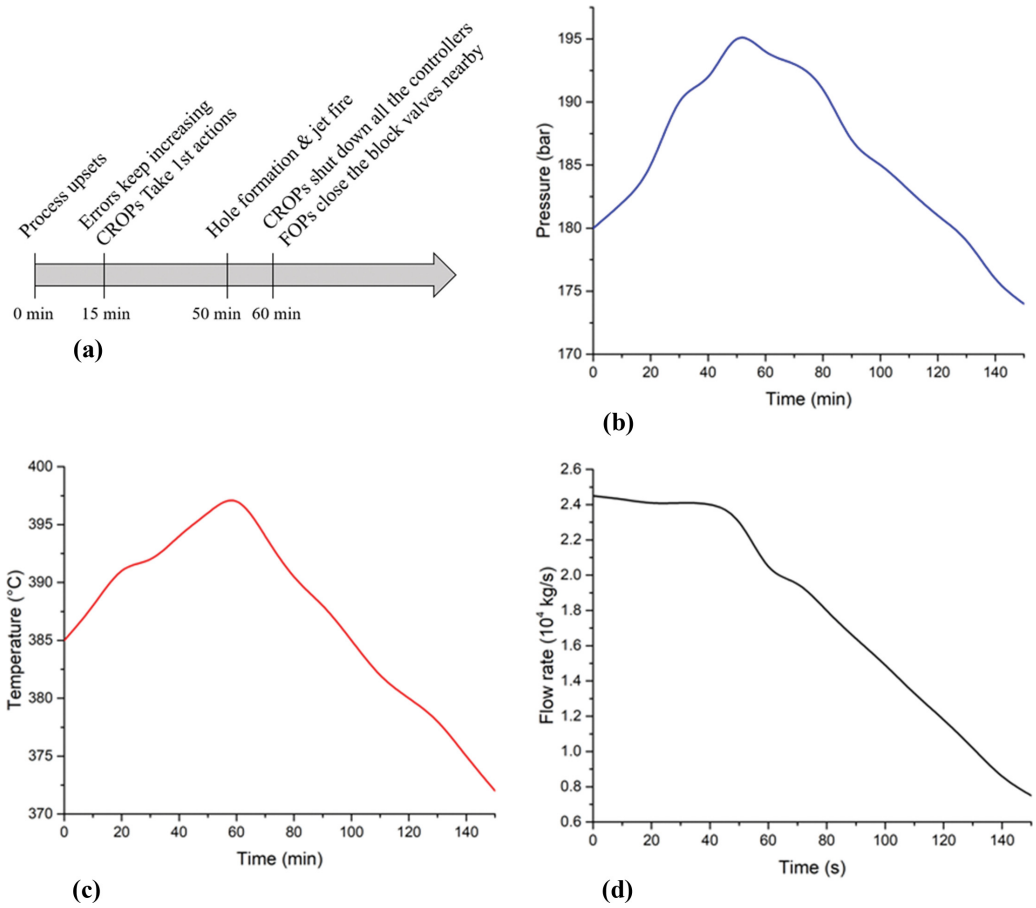

Fig. 6. Trend of process variables at B/V 1 during training. (a) Time-line of the events, (b) pressure, (c) temperature, (d) flow rate.

Fig. 4. Fig. 6(a) shows the time-line of the training scenario. The pressure and temperature increased abnormally in the initial stage of the training, whereas the flow rate remained at approximately the same value. Near the time step of 15 min, the CROPs set the controller mode to manual and closed the valve manually (1st action). However, since the error kept increasing as the predefined scenario, pressure and temperature continued to rise. At the time step of 50 min, the pressure reached the predefined release threshold and the leak began. The release rate was calculated by the discharge model of Eq. (1) in Section 2.1, the parameters of which were updated by the calculated values of the dynamic process simulation in real time. Once the leak began, the values of the process variables, e.g., pressure, temperature, and flow rate, began to decrease as part of the stream was released through the leak. At the time step of 60 min, the CROPs notified the FOPs of the accident site and initiated the shut-down procedure of the actuators (valves) in the DCS according to the training sequence in Section 3.1. Consequently, the values of the process variables continued to decrease, and if the FOPs reacted appropriately, the training ended. In this manner, the dynamic process simulation provided the CROPs and FOPs with a guideline on how to address emergencies in a real plant and served as a means of close communication between CROPs and FOPs in the emergency situation.

2. Accident Modeling Results

In Table 5 and Fig. 7, the mean and standard deviation of the

Table 5. Comparison of mean and standard deviation of different models

Model	Mean	Standard deviation
AE-NN	0.0124	0.0113
DAE-NN	0.00878	0.00864
DAE-DNN	0.00522	0.00345
DCAE-NN	0.00709	0.00715
DCAE-DNN	0.00328	0.00292
VAE-DNN	0.00298	0.00285
VAEDC-DNN	0.00272	0.00235

mean squared errors obtained from ten folds of each modelare shown. The mean squared error in each fold was obtained between x_{gen}^{test} and x^{test} for test data sets of 80 samples (x^{test}, v^{test}). The VAEDC-DNN model showed the highest performance (the lowest mean and standard deviation) of 0.00272 and 0.00235. The mean value of the worst case (AE-NN) was as low as 0.0124, but the standard deviation was as large as 0.0113, which means it is difficult to say that the training results were effectively generalized. The lowest mean and standard deviation signify that complex features were efficiently extracted by efficient mapping from the variable space to the latent space and the relationship between input and output is well inferred. It can be observed that when DNN was used, the

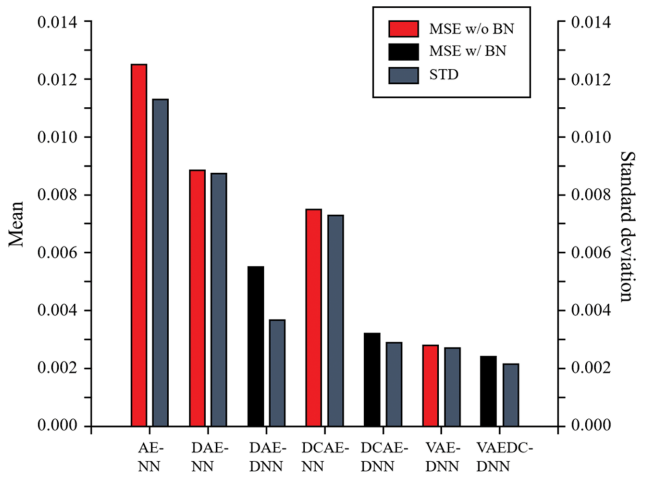

Fig. 7. Comparison of mean and standard deviation of different models.

performance of the models improved over the models with NN. However, the performance improved even when NN was used in the order of VAE, DCAE, DAE, and AE. This phenomenon indicates the great performance of dimensionality reduction, which directly denotes that the way in which nonlinear images are compressed serves to not only reduce the storage space but also to extract the features in suitable forms. The best performance was confirmed when VAE was combined with deep convolutional layers.

To identify the performance of the different surrogate model intuitively, the reconstructed images are presented in Fig. 8. In each column, randomly selected x_{gen}^{test} 2D contour images for AE-NN, DAE-DNN, DCAE-DNN, and VAEDC-DNN simulated from FLACS (CFD) are displayed. Owing to the characteristics of the nonlinear complexity of the images, the result differs in shape for each model, which indicates that it is difficult to reconstruct the overall macroscopic shape of the images using poor-performance dimensionality reduction models. This can be especially observed in the third and fourth columns in Fig. 8. In the surrogate models with dimensionality reduction, AE and VAE, excellent performance improvement can be identified. However, other models claim issues in predicting images. The AE-NN model is a right example of this. The approximate trends are reasonably similar; however, in the case of the fifth column, the prediction is significantly inaccurate. Reviewing the overall trend from Fig. 7 and Fig. 8, the introduction of BN contributed to advancement the surrogate model performance. The two best models, DCAE-DNN and VAEDC-DNN, showed best prediction performance compared with the other models, which shows the importance of convolutional layers. Between these models, the VAEDC-DNN model demonstrated superior performance, which can be seen in the first column where Q_{scaled} images were reconstructed with fine gradients of boundaries. The VAEDC-DNN model could detect features that were undetectable in the AEDC-DNN model.

3. AVR-based OTS Platform

Two types of information--process information from Aspen HYSYS and accident information from the VAEDC-DNN surrogate model--was combined to construct a platform to train both the CROPs and FOPs. As mentioned in Section 2.1, the training PAISE platform was introduced; the interface is displayed in Fig. 9(a). As can be identified in Fig. 1, PAISE serves not only to bridge the process model, accident model, and AVR, but also provides

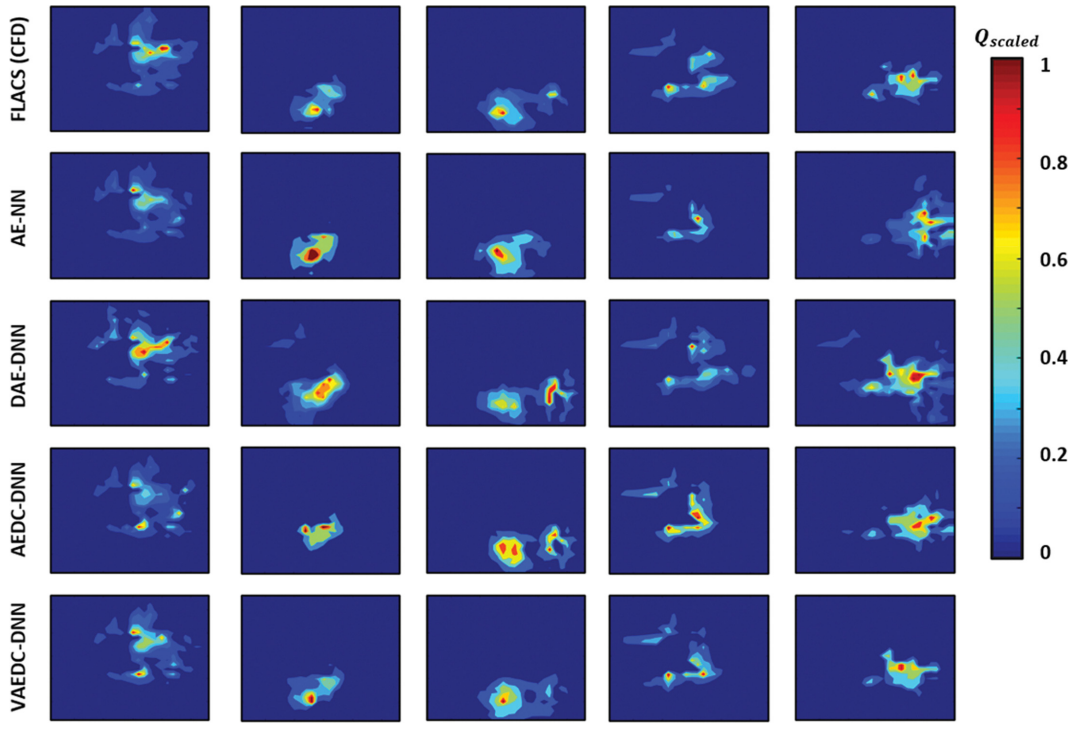

Fig. 8. Comparison of generated Q images by different models with original images by FLACS.

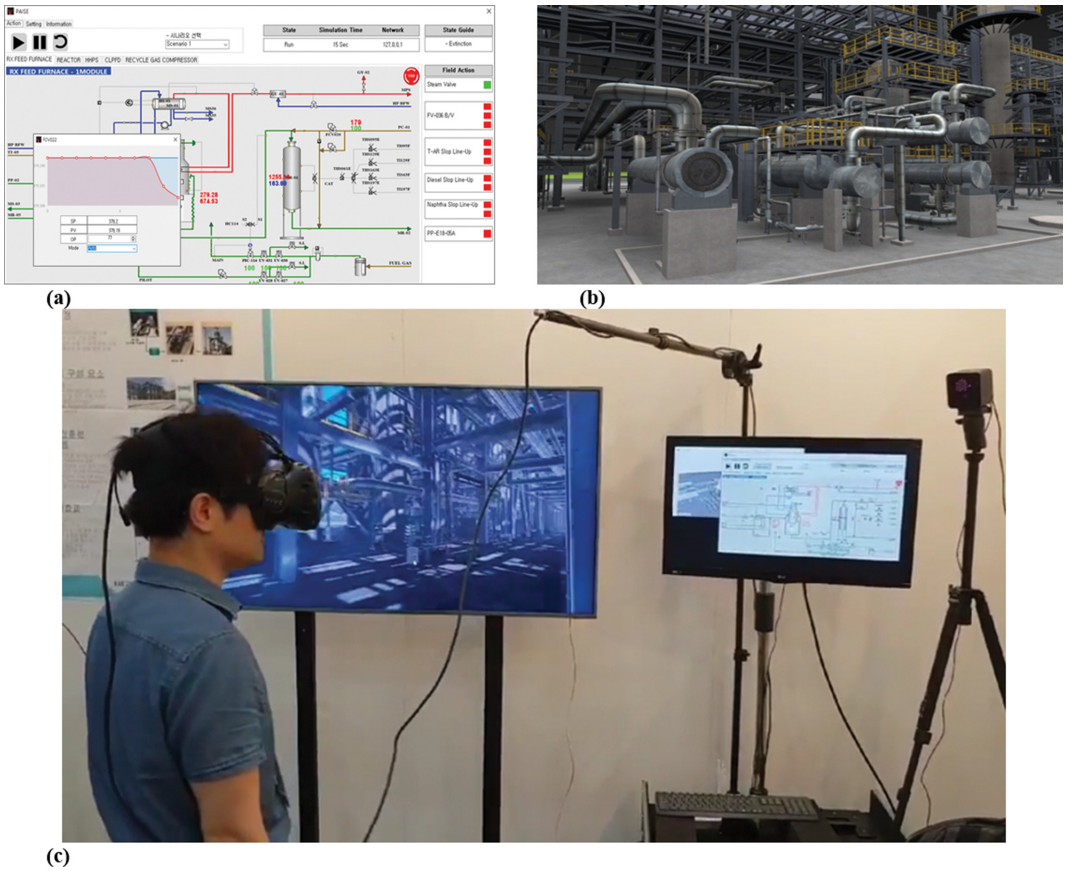

Fig. 9. AVR-based training environment. (a) DCS interface (PAISE), (b) VR interface, (c) training platform combined with DCS interface, VR interface, and other wearable devices.

process information to the CROPs. The interface of PAISE is similar to that of other conventional DCS-based OTSs. It indicates the trend of the process variables when the training scenario is initiated; the status of controllers and actuators (valves) can also be identified. To educate the FOPs, a VR interface was also developed, as displayed in Fig. 9(b). In the virtual environment, the trainees could walk around the plant and observe changes in the process equipment, e.g., pressure and temperature gauges, and operate valves.

When emergency situations occur, proper communication and cooperation of the CROPs and FOPs are essential. Therefore, a comprehensive AVR-based training platform was constructed, as indicated in Fig. 9(c); on the right is the PAISE interface for providing process information to the CROPs; on the left is the AVR with a combination of VR and other wearable gears such as acoustic, optical, and haptic devices for providing accident information to the FOPs. During training, as the training scenario evolves, the two types of operators interact with each other to prevent process upsets and accidents from propagating to a greater disaster.

Fig. 10 displays the training processes of a FOP with the demonstration version of the developed AVR-based OTS. During the training, the trainee experiences an augmented environment with the aid of an optical device as indicated in Fig. 10(a), and controller device as indicated in Fig. 10(b). The mapping of the accident result, i.e., lethality to the trainee, is in progress with OLE technology. When completed, the high degree-of-freedom for the train-

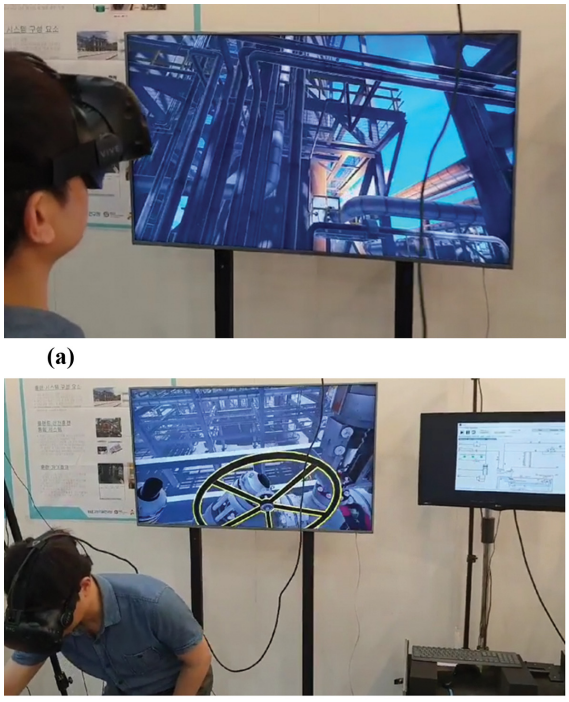

Fig. 10. Training examples (FOPs). (a) Jet fire image realization, (b) adjustment of haptic device during training.

ees' action and remarkably accurate process and accident information-based OTS are established.

CONCLUSION

In this study, a new OTS to train both CROPs and FOPs by coupling the dynamic process and accident models was introduced. The dynamic process model was constructed using Aspen HYSYS to provide the trainee with correct process variable information during the entire training. The physical and thermodynamic conditions were computed using the modified Peng-Robinson state model equation, and the pressure-flow equation was used for the calculation of the dynamic behavior. Consequently, the trend of the process variables was obtained quantitatively, then used as an input for the accident modeling. The accident model was constructed using the VAEDC-DNN surrogate model for real-time application of accident results in an AVR-based OTS. A VAEDC was introduced as a means of dimensionality reduction. The proposed model consists of two parts: VAEDC, dimensionality reduction of input images to the latent space, and DNN, regression of four-dimensional input space of wind speed, wind direction, release duration, and time steps. Using the constructed VAEDC-DNN model, the two-dimensional contour images were compressed to the latent space; the variable space was also mapped to the latent space. Other surrogate models were also constructed to compare the performance with using mean squared error. The VAEDC-DNN model demonstrated the best performance with a minimum mean squared error of 0.00278. It was proven that the VAEDC-DNN surrogate model excelled at extracting features from complex images. The high performance of the VAEDC-DNN surrogate model was then applied to the AVR-based OTS, where the target process was the HOD process, which is subject to frequent accidents because of the harsh operating conditions. Finally, an integrated platform with communication between the CROPs and FOPs, conducted with the aid of PAISE and an AVR platform, was constructed.

According to the proposed method, a versatile OTS can train both CROPs and FOPs simultaneously. First, it has a high degree-of-freedom in terms of trainees' actions. The change in the process variables from the actions of the CROPs in DCS is calculated by process simulation in real time; the change in accident results, e.g., Q, from the actions of the FOPs, is also calculated in real time with the high-performance VAEDC-DNN model. Second, a better training effect over conventional OTSs can be realized, especially for the FOPs because the training scenario is initiated with random inputs of wind speed and wind direction, thereby providing diverse accident results. Lastly, simulation-based process information of the surrogate model-derived accident information ensures high accuracy for the trainees, consequently helping reduce the damage of potential catastrophic accidents in advance.

ACKNOWLEDGEMENT

This research was supported by a grant (19IFIP-B087592-06) from the Smart Civil Infrastructure Research Program funded by the Ministry of Land, Infrastructure and Transport (MOLIT) of the Korean government and the Korea Agency for Infrastructure Technology Advancement (KAIA), a grant (NRF-2019R1A2C1085081) from the National Research Foundation of Korea (NRF) funded by the Korean government (MSIT), and Yullin Technologies Co., Ltd.

NOMENCLATURE

C_{disc}	: discharge coefficient
A	: cross-sectional area of orifice [m^2]
γ	: specific heat ratio
ρ	: density [kg/m^3]
Q	: total heat flux [W/m^2]
Δx_i	: length of cell in *i*-direction
Δt	: simulation time step
K_c	: controller gain
τ_i	: integral time
z	: latent space
N_z	: number of latent variables
v	: variable space
N_v	: the number of variables
N_{train}	: the number of training datasets

Abbreviations

OTS	: operator training system
DCS	: distributed control system
CROP	: control room operator
FOP	: field operator
VR	: virtual reality
AVR	: augmented virtual reality
CFD	: computational fluid dynamics
AE	: Autoencoder
VAE	: variational autoencoder
CNN	: convolutional neural network
DNN	: deep neural network
VAEDC	: variational autoencoder with deep convolutional layers
HOD	: heavy oil desulfurization
PAISE	: process and accident interactive simulation engine

REFERENCES

1. M. M. Maresh, *The aftermath of a deadly explosion: A rhetorical analysis of crisis communication as employed by British Petroleum and Phillips Petroleum*, in, Texas Tech University (2006).
2. A. Antonovsky, C. Pollock and L. Straker, *Human Factors*, **56**, 306 (2014).
3. T. A. Kletz, *Process Saf. Prog.*, **17**, 196 (1998).
4. S. A. M. Naqvi, M. Raza, S. Ghazal, S. Salehi, Z. Kang and C. Teodoriu, *Process Saf. Environ. Prot.*, **138**, 220 (2020).
5. Z. Ahmad, D. S. Patle and G. P. Rangaiah, *Process Saf. Environ. Prot.*, **99**, 55 (2016).
6. L. Marcano, F. A. Haugen, R. Sannerud and T. Komulainen, *Saf. Sci.*, **115**, 414 (2019).
7. S. Morgan, S. Sendelbach and W. Stewart, *Hydrocarbon processing*, United States (1994).
8. P. Rutherford, W. Persad and M. Lauritsen, *Hydrocarbon processing*, United Sates (2003).

9. C. Siminovich and S. Joao, *Procedia Eng.*, **83**, 215 (2014).
10. S. H. Yang, L. Yang and C. H. He, *Process Saf. Environ. Prot.*, **79**, 329 (2001).
11. P. V. Carvalho, M. C. Vidal and E .F. de Carvalho, *Human Factors and Ergonomics in Manufacturing & Service Industries*, **17**, 43 (2007).
12. M. Cha, S. Han, J. Lee and B. Choi, *Fire Saf. J.*, **50**, 12 (2012).
13. J. Cibulka, P. Mirtaheri, S. Nazir, D. Manca and T. M. Komulainen, Virtual Reality Simulators in the Process Industry: A Review of Existing Systems and the Way Towards ETS, in: Proceedings of The 9th EUROSIM Congress on Modelling and Simulation, EUROSIM 2016, The 57th SIMS Conference on Simulation and Modelling SIMS 2016, Linköping University Electronic Press, 2018, pp. 495-502.
14. D. Manca, S. Brambilla and S. Colombo, *Adv. Eng. Software*, **55**, 1 (2013).
15. S. R. Hanna, M. J. Brown, F. E. Camelli, S. T. Chan, W. J. Coirier, O. R. Hansen, A. H. Huber, S. Kim and R. M. Reynolds, *Bull. Am. Meteorol. Soc.*, **87**, 1713 (2006).
16. S. R. Hanna, O. R. Hansen and S. Dharmavaram, *Atmos. Environ.*, **38**, 4675 (2004).
17. K. J. Long, F. J. Zajaczkowski, S. E. Haupt and L. J. Peltier, *JCP*, **4**, 881 (2009).
18. P. Middha, O. R. Hansen, J. Grune and A. Kotchourko, *J. Hazard. Mater.*, **179**, 84 (2010).
19. K. Palmer and M. Realff, *Chem. Eng. Res. Des.*, **80**, 773 (2002).
20. T. Chen, K. Hadinoto, W. Yan and Y. Ma, *Comput. Chem. Eng.*, **35**, 502 (2011).
21. A. Widodo and B.-S. Yang, *Mechanical Systems and Signal Processing*, **21**, 2560 (2007).
22. M. Fauvel, J. Chanussot and J. A. Benediktsson, *Pattern Recognition*, **45**, 381 (2012).
23. I. A. Udugama, C. L. Gargalo, Y. Yamashita, M. A. Taube, A. Palazoglu, B. R. Young, K. V. Gernaey, M. Kulahci and C. Bayer, *Ind. Eng. Chem. Res.*, **59**, 15283 (2020).
24. O. T. Kajero, T. Chen, Y. Yao, Y.-C. Chuang and D. S. H. Wong, *J. Taiwan Inst. Chem. Engineers*, **73**, 135 (2017).
25. J. Masci, U. Meier, D. Cireşan and J. Schmidhuber, *Stacked convolutional auto-encoders for hierarchical feature extraction*, in: International Conference on Artificial Neural Networks, Springer, 52 (2011).
26. J. Geng, J. Fan, H. Wang, X. Ma, B. Li and F. Chen, *IEEE Geoscience and Remote Sensing Letters*, **12**, 2351 (2015).
27. D. P. Kingma and M. Welling, *Auto-encoding variational bayes*, arXiv preprint arXiv:1312.6114 (2013).
28. J. Na, K. Jeon and W. B. Lee, *Chem. Eng. Sci.*, **181**, 68 (2018).
29. A. Géron, *Hands-on machine learning with Scikit-Learn and TensorFlow: concepts, tools, and techniques to build intelligent systems*, O'Reilly, United States (2017).
30. S. Ioffe and C. Szegedy, *Batch normalization: Accelerating deep network training by reducing internal covariate shift*, arXiv preprint arXiv:1502.03167 (2015).
31. D. P. Kingma and J. Ba, *Adam: A method for stochastic optimization*, arXiv preprint arXiv:1412.6980 (2014).
32. D.-Y. Yun, S.-K. Seo, U. Zahid and C.-J. Lee, *Appl. Sci.*, **10**, 4005 (2020).
33. G. A. Melhem, R. Saini and B. M. Goodwin, *Fluid Phase Equilib.*, **47**, 189 (1989).
34. M. Stein, *Technometrics*, **29**, 143 (1987).
35. J. Maltby, S. Phipps and V. Singleton, US Patent, 6,202,100 B1 (2001).
36. H. W. Witlox, M. Fernández, M. Harper, A. Oke, J. Stene and Y. Xu, *J. Loss Prevent. Proc. Ind.*, **55**, 457 (2018).
37. A. Géron, *Hands-on machine learning with Scikit-Learn, Keras, and TensorFlow: Concepts, tools, and techniques to build intelligent systems*, O'Reilly, United States (2019).
38. C. Ko, *Risk Management of Chemical Processes Using Dynamic Simulation and CFD-based Surrogate Model Approach*, in, Seoul National University (2020).